Acta Cryst E CRYSTALLOGRAPHIC COMMUNICATIONS

ISSN 2056-9890

Crystal structures of *N*-[4-(trifluoromethyl)-phenyl]benzamide and *N*-(4-methoxyphenyl)-benzamide at 173 K: a study of the energetics of conformational changes due to crystal packing

Wayne H. Pearson,*‡ Joseph J. Urban, Amy H. Roy MacArthur, Shirley Lin and Dylan W. L. Cabrera

Chemistry Department, United States Naval Academy, 572 Holloway Rd, Annapolis, MD 21402, USA. *Correspondence e-mail: waynehp21662@gmail.com

Received 5 October 2021
Accepted 27 January 2022

Edited by M. Weil, Vienna University of Technology, Austria

‡ Retired.

Keywords: crystal structure; intermolecular forces; aryl amides; DFT calculations; Hirshfeld surfaces; molecular interaction energies.

CCDC references: 2144924; 2144923

Supporting information: this article has supporting information at journals.iucr.org/e

As a part of our study of the syntheses of aryl amides, the crystal structures of two benzamides were determined from single-crystal X-ray data at 173 K. Both crystal structures contain molecular units as asymmetric units with no solvent in the unit cells. Crystal structure I, **TFMP**, is the result of the crystallization of *N*-[4-(trifluoromethyl)phenyl]benzamide, $C_{14}H_{10}F_3NO$. Crystal structure II, **MOP**, is composed of *N*-(4-methoxyphenyl)benzamide, $C_{14}H_{13}NO_2$, units. **TFMP** is triclinic, space group $P\overline{1}$, consisting of two molecules in the unit cell related by the center of symmetry. **MOP** is monoclinic, space group $P2_1/c$, consisting of four molecules in the unit cell. Both types of molecules contain three planar regions; a phenyl ring, an amide planar region, and a *para*-substituted phenyl ring. The orientations of these planar regions within the asymmetric units are compared to their predicted orientations, in isolation, from DFT calculations. The aryl rings are tilted approximately 60° with respect to each other in both experimentally determined structures, as compared to 30° in the DFT results. These conformational changes result in more favorable environments for N—H···O hydrogen bonding and aryl ring π-stacking in the crystal structures. Intermolecular interactions were examined by Hirshfeld surface analysis and quantified by calculating molecular interaction energies. The results of this study demonstrate that both hydrogen bonding and dispersion are essential to the side-by-side stacking of molecular units in these crystal structures. Weaker dispersion interactions along the axial directions of the molecules reveal insight into the melting mechanisms of these crystals.

1. Chemical context

Numerous methodologies have been developed to form amide C—N bonds due to their prevalence in biomolecules, such as peptides and proteins, and in synthetic targets (Seward & Jakubke, 2002; Greenberg *et al.*, 2000). In particular, aryl amides can be found in a variety of pharmaceutical drugs and in polymers such as Kevlar™ (Masse *et al.*, 1998; Evano *et al.*, 2004, 2008; Satyanarayana *et al.*, 2007; Tanner *et al.*, 1989). A series of aryl amides were synthesized and isolated during the development of a copper-mediated concurrent tandem catalytic methodology for the amidation of aryl chlorides (Chang *et al.*, 2019). The crystal structures of two of these aryl amides, derived from the cross-coupling of either 4-chlorobenzotrifluoride or 4-chloroanisole with benzamide, are reported here.

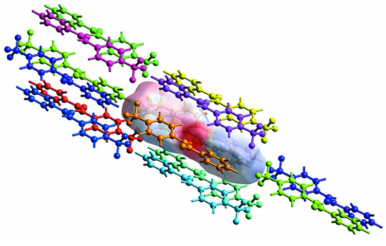

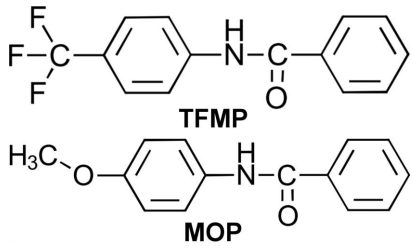

2. Structural commentary

The reported compounds are substituted benzamides containing a *para*-substituted phenyl ring in place of one of the hydrogen atoms of the amide nitrogen. In both crystal structures, the asymmetric unit is a single molecule of the compound. Crystal structure I, **TFMP**, contains an asymmetric unit with a trifluoromethylphenyl ring. Crystal structure II, **MOP**, has an asymmetric unit with a methoxyphenyl ring. The molecular structures in the form of ellipsoid plots are shown in Fig. 1. There is nothing remarkable about the individual bond lengths, bond angles, or planarity of the aryl rings in these molecules.

Fig. 2 contains the unit cells for both crystal structures. Both molecules assume chiral configurations. Because the space groups are centrosymmetric, the unit-cell contents are racemic mixtures containing the enantiomers of the molecules in symmetry-related positions. In both crystal structures, the molecules align along the molecular axes. This alignment results in the long axes in both unit cells, c = 14.415 (3) Å in **TFMP** and a = 26.783 (2) Å in **MOP**.

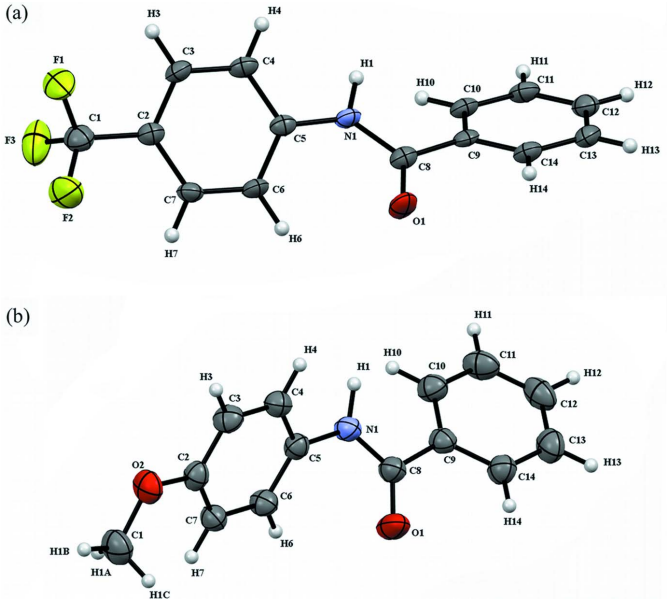

Figure 1
The molecules present in the asymmetric units in (*a*) **TFMP** and (*b*) **MOP**. Displacement ellipsoids are drawn at the 50% probability level. Hydrogen atoms are represented by spheres of 0.20 Å radius.

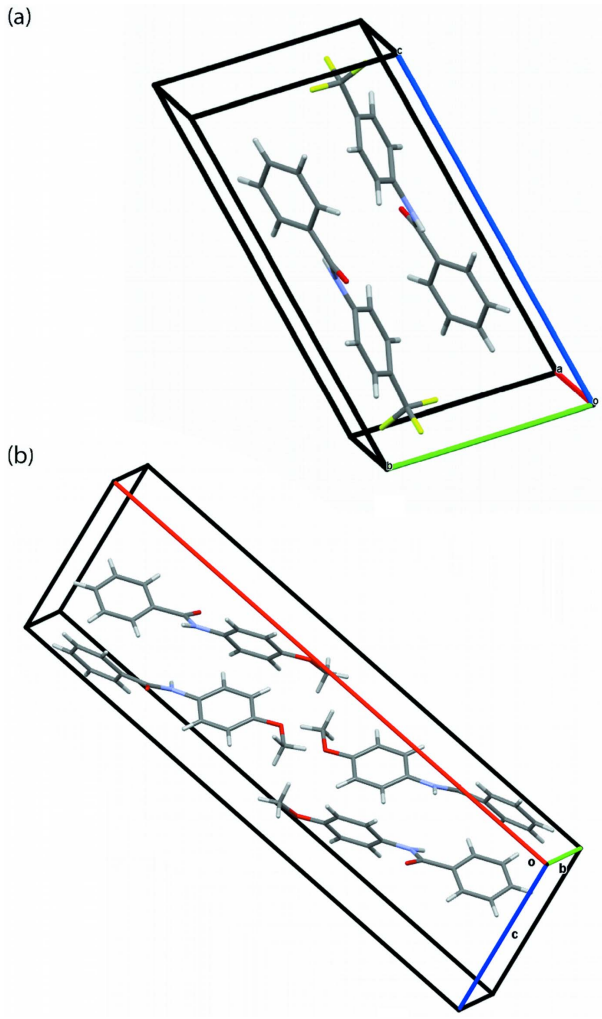

Figure 2
Unit-cell packing of (*a*) **TFMP** and (*b*) **MOP**.

Both molecules contain three planar regions; a phenyl ring, an amide linkage, and the *para*-substituted phenyl ring. Rotation of the rings relative to each other can lead to conformations that exist in the crystal structures that differ from the native molecular conformations. The relationship between the conformations of organic molecules and crystal structures has been reported extensively and summarized in the review article by Cruz-Cabeza & Bernstein (2014). Tilt angles were determined by comparing the angles between normals to least-squares planes as defined by the non-hydrogen atoms in a planar region. Significant tilt angles exist between the planar regions in both molecules in the experimentally determined structures as shown in Fig. 3.

3. DFT calculations and results for isolated molecules

Quantum-chemical density functional theory (DFT) calculations were performed to find the conformations of global minimum energy for the two molecules in isolation. Calculations were performed with the *GAUSSIAN09* (Frisch *et al.*, 2016) program suite on DoD High Performance Moderniza-

tion resources. Initial conformer searching was performed at the molecular mechanics level with the MMFF force field as implemented in *SPARTAN* molecular modeling software (Wavefunction, 2014). Viable structures were then subjected to complete geometry optimizations in *GAUSSIAN09* at the M06-2X/6-31+G(d) level (Zhao & Truhlar, 2008). Frequency calculations were performed at M06-2X/6-31+G(d) to confirm that all stational points were minima. Comparisons of bond lengths and angles between the experimentally determined structures and the DFT calculations can be found in the supporting information.

Tilts of the planar regions from the DFT calculations are also shown in Fig. 3. The amide plane/phenyl ring angles are approximately 29° in the experimental results and 27° in the calculated molecules. In the experimentally determined structures, the angles between *para*-substituted phenyl rings and the amide planes are 31.4 (2)° in **TFMP** and 38.4 (4)° in **MOP**. The DFT calculations yield much smaller angles of 8.5 and 7.9°, respectively. These results indicate that the conformational change due to crystal packing in both molecules is primarily due to ring tilts around the N1—C5 bonds while the rings joined by C8—C9 bonds are essentially oriented the same as in the isolated molecules. A search of benzamides in the Cambridge Structural Database (version 2020.3; Groom *et al.*, 2016) revealed a number of compounds with similar phenyl ring/amide plane tilts. For example, *N*-phenylbenzamide (Wang *et al.*, 2014), *N*-(4-hydroxyphenyl)benzamide (Tothadi & Desiraju, 2012), benzamide (Blake & Small, 1972) and *N*-(4-nitrophenyl)benzamide (du Plessis *et al.*, 1983) all possess amide plane/phenyl ring angles between 28 and 31°. A likely explanation for the consistent amide plane/phenyl ring tilt would be the balance of the attractive O1···H14 interactions and the repulsive interactions of H1···H10.

Additional DFT calculations were performed to determine approximate energy differences between the molecules in isolation and conformations found in the crystal structures. To best approximate the conformations in the experimentally determined structures, dihedral angles around the amide linkage were constrained to crystallographic values while all other geometrical parameters were allowed to vary. Tilt angles between phenyl and *para*-substituted phenyl rings are in good agreement between the X-ray models and DFT calculations. For **TFMP**, the angles are 59.7 (1)° in the crystal structure and 59.6° in the DFT calculation. For **MOP**, the angles are 67.4 (1)° in the crystal structure and 66.8° in the DFT calculation. The results of the DFT calculations show that the energies of the conformations in the experimentally determined structures are slightly above those in the isolated molecules, *viz*. 3.2 kJ mol^{-1} higher for **TFMP** and 2.5 kJ higher for **MOP**.

4. Supramolecular features

Close packing in both crystal structures is the result of hydrogen bonding, dipole interactions and dispersion. Hydrogen bonds were revealed by using the HTAB command in *SHELXL* (Sheldrick, 2015*b*) and verified using *PLATON*

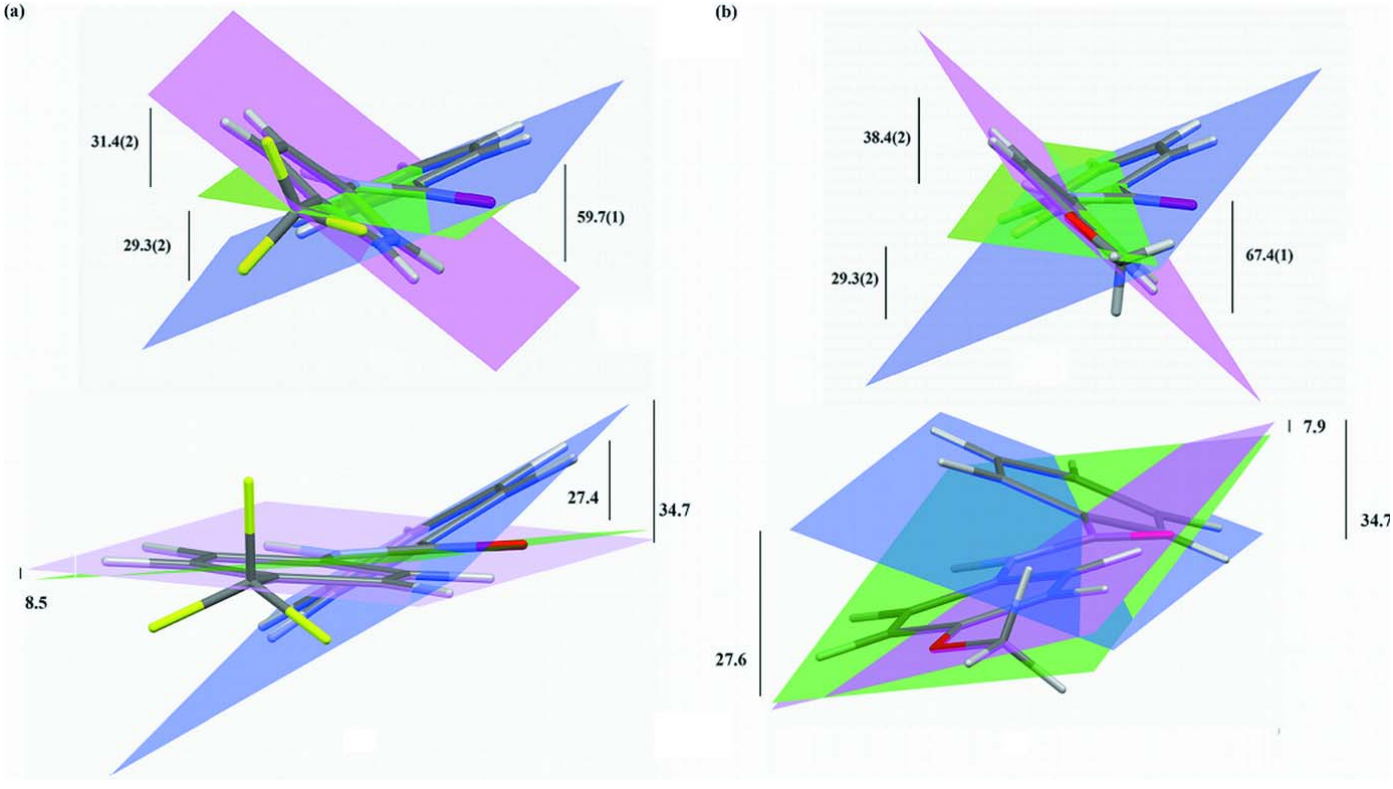

Figure 3
Views of orientations of planar regions and their dihedral angles (in °) from experimental results (top) and DFT calculations (bottom) for (*a*) **TFMP** and (*b*) **MOP**. Blue = phenyl ring; green = amide plane; mauve = *para*-substituted phenyl ring.

Table 1
Hydrogen-bond geometry (Å, °) for **TFMP**.

D—H···A	D—H	H···A	D···A	D—H···A
C6—H6···O1	0.95	2.44	2.938 (4)	112
C4—H4···O1^{i}	0.95	2.57	3.240 (4)	128
N1—H1···O1^{i}	0.99 (1)	2.23 (2)	3.138 (3)	151 (3)

Symmetry code: (i) $x-1, y, z$.

Table 2
Hydrogen-bond geometry (Å, °) for **MOP**.

D—H···A	D—H	H···A	D···A	D—H···A
C6—H6···O1	0.95	2.49	2.912 (2)	107
N1—H1···O1^{i}	0.96 (1)	2.16 (1)	3.108 (2)	166 (2)

Symmetry code: (i) $x, y-1, z$.

(Spek, 2020). The H···O contacts are listed in Tables 1 and 2 and shown in Fig. 4. There is only one type of N—H···O interaction in both crystal structures, in the direction parallel to the *a* axis for **TFMP** and the *b* axis in **MOP**. There are non-classical carbon-based hydrogen bonds that exist as intramolecular interactions (C6—H6···O1) in both crystal struc-

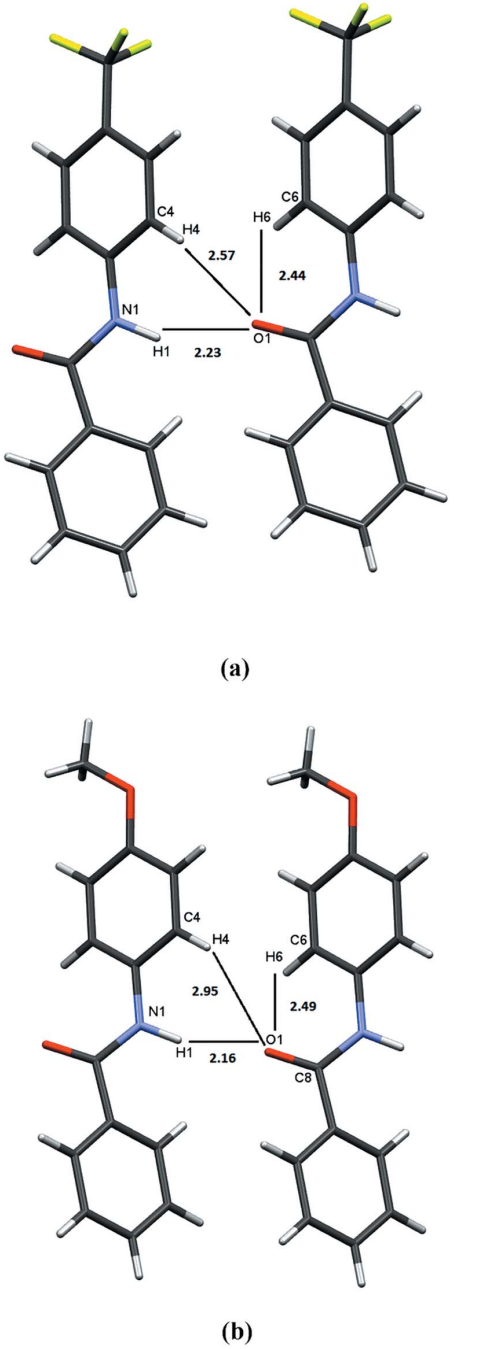

Figure 4
Hydrogen bonding contacts (in Å) in (*a*) **TFMP** and (*b*) **MOP**.

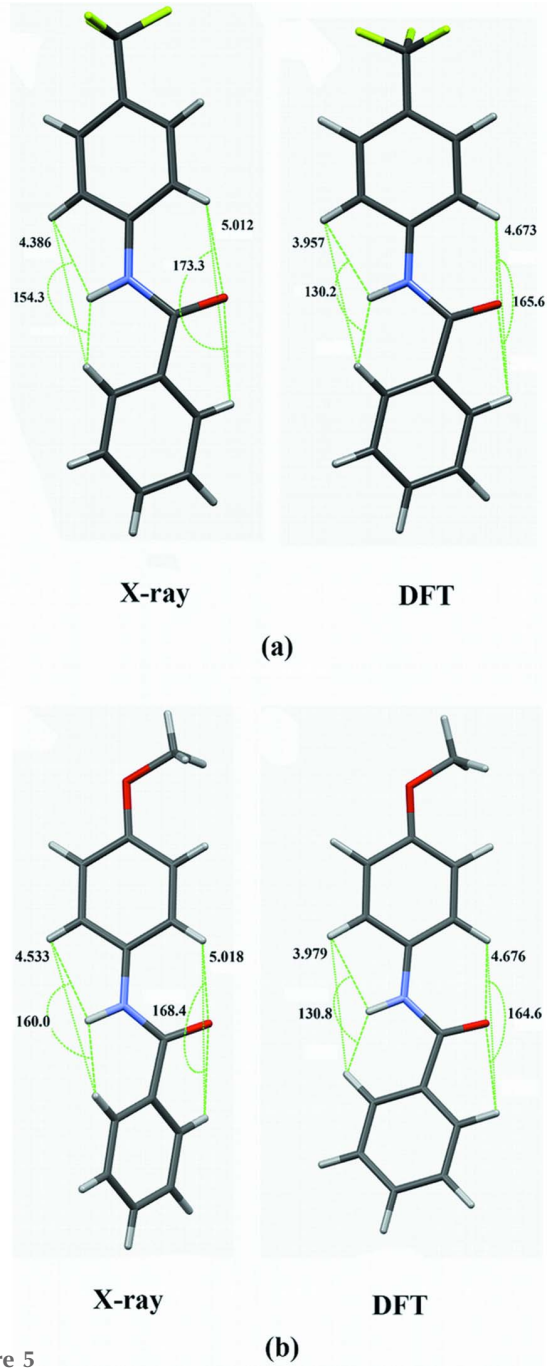

Figure 5
Comparison of hydrogen-bonding environments (in Å) from X-ray results and DFT calculations for (*a*) **TFMP** and (*b*) **MOP**.

tures and intermolecular contacts (C4—H4···O1) in **TFMP** only. The longer H4···O1 contact in **MOP** (2.95 Å) is a result of the larger ring twist angle between the *para*-substituted phenyl ring and the amide linkage in **MOP**, 38.4° *versus* 31.4° in **TFMP**.

Comparisons of hydrogen-bonding regions from the experimentally determined structure and DFT results are shown in Fig. 5 for **TFMP** and **MOP**. In both cases, the molecules in the crystal structures have a more open environment with larger angles around the donor and acceptor sites and larger donor and acceptor cavities. The increased planar tilt between *para*-substituted phenyl rings and amide planes is a contributor to the more open hydrogen-bonding environments in the experimentally determined structures.

The increased tilt angles between the amide and *para*-substituted phenyl planes also facilitate the π-stacking in both crystal structures (Table 3). Neighboring environments around aryl rings are shown in Fig. 6. Each aryl ring has close contacts with six other aryl rings. In **TFMP**, there are contacts between trifluoromethylphenyl rings and phenyl rings. In **MOP**, phenyl rings have close contacts with phenyl rings while methoxyphenyl rings have contacts with other methoxyphenyl rings on neighboring molecules. There are a total of six interactions surrounding each aryl ring, with four T-shaped interactions and two being a parallel displacement of rings. Neighboring molecules that have parallel displaced rings are involved in the N—H···O hydrogen bonding. A quantitative discussion of the π stacking geometries based upon the approach of Banerjee *et al.* (2019) can be found in the supporting information.

Intermolecular interactions in the remaining axial direction, *c* in **TFMP** and *a* in **MOP**, are shown in Fig. 7. In **TFMP**, the axial interactions are between a trifluoromethyl group on one molecule and a phenyl ring on its neighbor. In **MOP**, the closest interactions are of two types, methoxyphenyl–methoxyphenyl interactions and phenyl–phenyl interactions. The neighboring phenyl rings have a centroid distance of 6.4 Å and do not overlap.

Table 3
π-stacking parameters for **TFMP** and **MOP**.

All distances are in Å with estimated uncertainties of 0.004. Angles are in ° with estimated uncertainties of 0.2.

Centroid	Normal	Offset	Twist angle
TFMP – surrounding both rings			
4.774	4.672	0.982	59.7
4.718	4.649	0.804	59.7
4.711	4.646	0.780	59.7
4.698	4.611	0.900	59.7
5.361	2.666	4.651	0.0
MOP – surrounding phenyl rings			
4.781	4.757	0.478	64.6
4.901	4.875	0.504	64.6
5.248	2.802	4.437	0.0
MOP – surrounding methoxyphenyl rings			
4.849	4.658	1.348	68.1
4.831	4.64	1.345	68.1
5.248	2.938	4.349	0.0

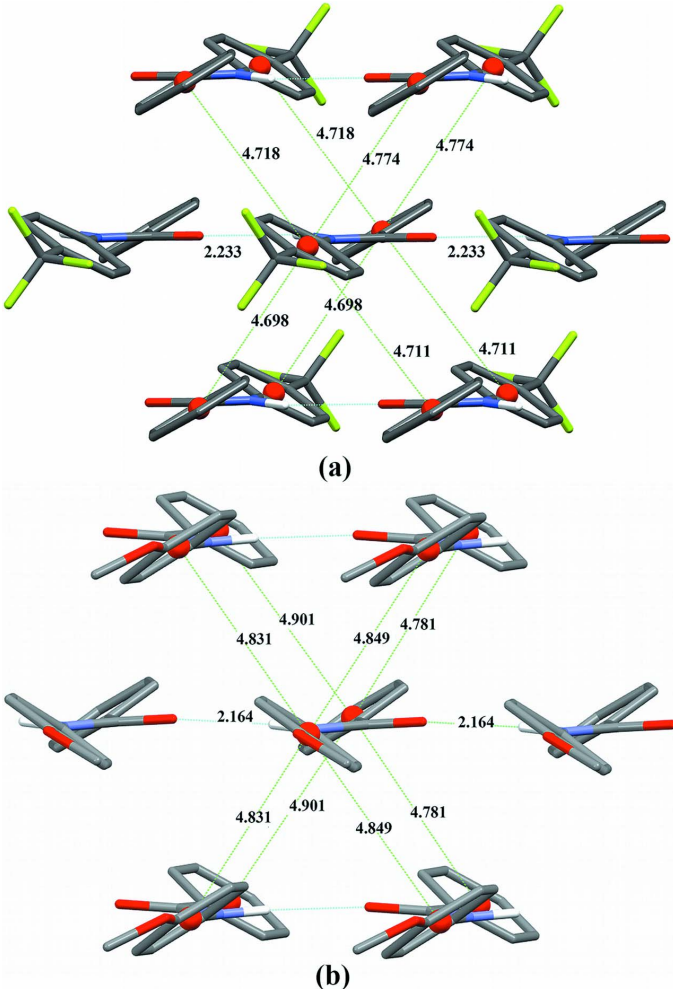

Figure 6
Hydrogen bonding and π-stacking (in Å) in (*a*) **TFMP** and (*b*) **MOP** (s.u.'s for centroid distances are approximately 0.005 Å). Riding H atoms are omitted for clarity.

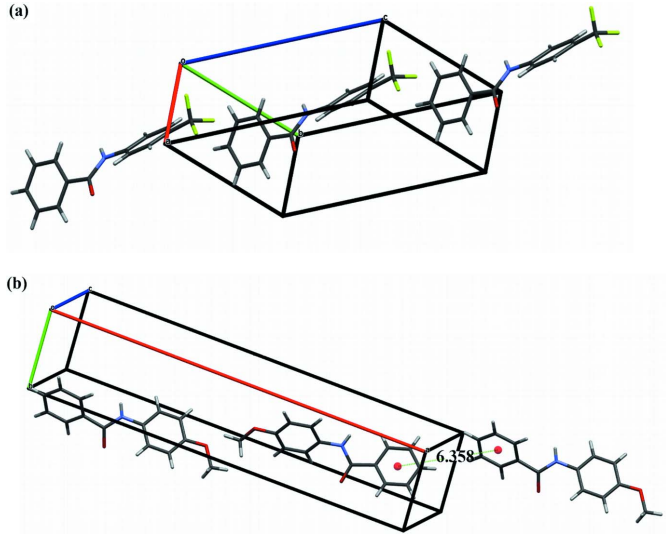

Figure 7
View of contacts (in Å) along the molecular axes in (*a*) **TFMP** and (*b*) **MOP**.

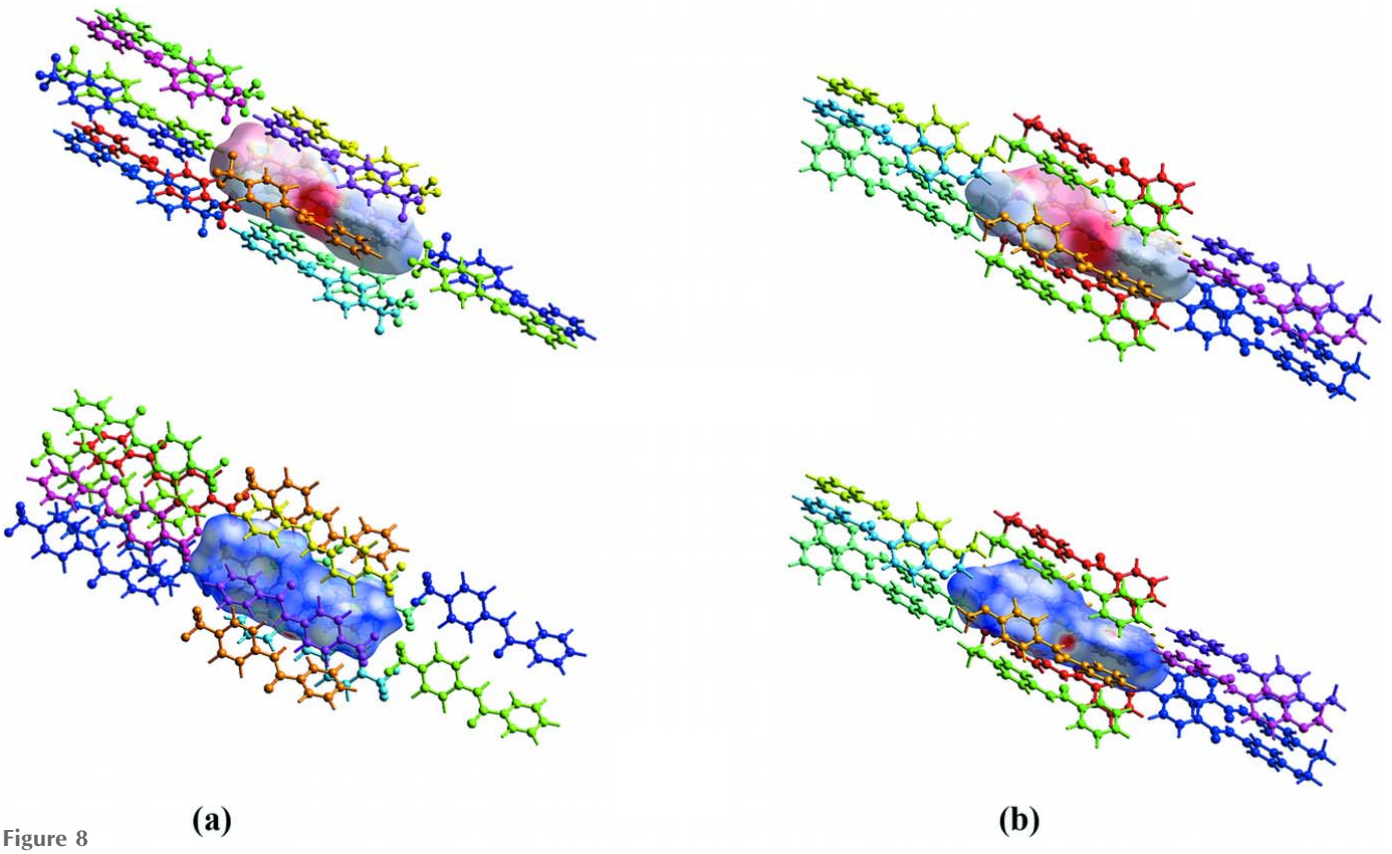

Figure 8
Intermolecular interaction energies and Hirshfeld surfaces with electrostatic potential (top) and d_{norm} (bottom) plots are shown for (*a*) **TFMP** and (*b*) **MOP**. Scales for electrostatic potential are red (−0.0788) to blue (0.1227) au for **TFMP** and red (−0.0875) to blue (0.1219) au for **MOP**. Scales for d_{norm} are red (−0.2905) to blue (0.9711) for **TFMP** and red (−0.3719) to blue (1.1524) for **MOP**. The color code for molecular interactions is shown in Fig. 9.

5. Hirshfeld surfaces and molecular pair interaction energies

To further examine the supramolecular environments, Hirshfeld surfaces and molecular pair interaction energies were calculated for both crystal structures. All of these calculations were performed using the CE-B3LYP method *via* the *TONTO* program (Jayatilaka & Grimwood, 2003) as implemented in *CrystalExplorer17* (Spackman *et al.*, 2021). Interaction energies use benchmarked models based upon B3LYP/6-31G(d,p) functionals, coupled with appropriate scale factors for electrostatic, polarization, dispersion and repulsion energies. The CE-B3LYP model is benchmarked against B3LYP-D2/6-31G(d,p) counterpoise-corrected energies and has been found to give very good agreement with CCSD(T)/CBS (Turner *et al.*, 2014).

Hirshfeld surfaces and molecular interaction energies are shown in Fig. 8. The neighboring molecules fall within 3.8 Å from the molecule inside the Hirshfeld surface. The color coding keys and scaled energies are found in Fig. 9. Although the energy values are reported to 0.1 of a kJ mol^{-1}, the authors of *CrystalExplorer17* recommend that the reliability is on the order of 1 kJ mol^{-1}. As a result, the total interaction energies (E_{tot}) are rounded to a kJ mol^{-1}. As expected, the major E_{tot} energies occur for the side-by-side interactions for **TFMP** (# 1–5) and **MOP** (# 1–3). The percent contributions to the $E_{attract}$ from the electrostatic, polarization and dispersion components are reported. Dispersion is the major attractive interaction in both crystal structures. For molecules with hydrogen-bonded close contacts and for some interactions along the molecular axes directions, the electrostatic energies are roughly equal to the dispersion energies. Videos showing 360° rotations of the static views in Fig. 8 can be found in the supporting information.

In Fig. 8, the electrostatic potentials, plotted on the Hirshfeld surfaces, show regions of negative charge (red) and positive charge (blue) for both compounds. For **TFMP**, in Fig. 8*a*, the electrostatic interaction of the hydrogen-bonding region is evident but so is the head-to-tail stacking of neighboring molecules due to the attraction of negative trifluoromethyl groups with neighboring positive phenyl hydrogens. For **MOP**, in Fig. 8*b*, the electrostatic interaction of the hydrogen bonding is apparent but the polar nature in the remaining segments of the molecule is localized in the methoxy group, contributing to the preference for association of methoxyphenyl rings in the crystal structure.

Fig. 8 also includes Hirshfeld surfaces with d_{norm} surface plots. Intermolecular contacts less than a van der Waals contact are colored red, roughly equal contacts are white, and contacts longer than a van der Waals contact are blue. White or red contacts should indicate some degree of intermolecular interaction of inner and outer atoms at those positions on the Hirshfeld surfaces. Specific close contacts are shown in the supporting information.

TFMP									%E_attract	%E_attract	%E_attract
Interaction	Color	R	E_ele	E_pol	E_dis	E_rep	E_tot	E_attract	E_ele	E_pol	E_dis
1		5.36	-31.7	-5.1	-34.3	24.5	-47	-71	45	7	48
2		5.26	-13.6	-1.6	-39.4	14.5	-40	-55	25	3	72
3		5.17	-12.4	-2.2	-42.2	18.5	-38	-57	22	4	74
4		6.32	-13.4	-1.3	-37.0	14.7	-37	-52	26	2	72
5		6.28	-10.9	-2.1	-37.5	18.0	-33	-50	22	4	74
6		10.68	-0.6	-0.4	-9.5	1.7	-9	-10	6	4	90
7		14.43	-3.3	-0.4	-7.8	3.0	-8	-11	29	3	68
8		14.42	-2.6	-0.2	-3.4	1.0	-5	-6	42	4	54
9		12.30	2.3	-0.2	-4.6	0.4	-2	-5	0	5	95
10		11.95	0.1	-0.1	-1.7	0.0	-2	-2	0	4	96
11		13.39	-0.1	-0.1	-1.2	0.0	-1	-1	8	5	87

MOP									%E_attract	%E_attract	%E_attract
Interaction	Color	R	E_ele	E_pol	E_dis	E_rep	E_tot	E_attract	E_ele	E_pol	E_dis
1		5.25	-35.4	-6.4	-33.3	23.9	-51	-75	47	8	44
2		4.58	-11.6	-2.2	-38.8	16.3	-36	-53	22	4	74
3		5.15	-9.4	-1.3	-32.2	13.7	-29	-43	22	3	75
4		13.99	-8.0	-0.9	-7.3	4.8	-11	-16	49	5	45
5		13.45	-1.3	-0.4	-7.4	2.2	-7	-9	14	5	81
6		13.38	-2.1	-0.1	-7.8	3.5	-7	-10	21	1	77
7		14.20	-0.3	-0.2	-5.9	2.2	-4	-6	5	3	92
8		14.76	0.2	-0.1	-3.0	0.9	-2	-3	0	5	95
9		14.17	-0.1	-0.1	-1.5	0.1	-2	-2	6	4	89

R = distance between molecular centers	E_ele = electrostatic contribution	E_pol = polarization contribution
E_dis = dispersion contribution	E_rep = repulsion contribution	E_tot = total energy of interaction
E_attract = sum of negative contributions		

Figure 9
Key for the intermolecular interaction energies for **TFMP** and **MOP**. Energy units are kJ mol^{-1}.

Insight into the melting process for these crystals can be obtained from the energy analysis. Melting of these crystals would require overcoming the weak intermolecular interactions along the direction of the molecular axes. In the case of **TFMP**, the energy required would be on the order of 8–9 kJ mol^{-1} (interactions #6 and #7 in Fig. 9). In **MOP**, the energy required would only be around 7 kJ mol^{-1} (interactions #5 and #6). Although these energy values are internal energies and not enthalpies, they are reasonable values for heats of fusion and correlate with the melting points of the two crystal structures, 478 K for **TFMP** and 425 K for **MOP** (Chang *et al.*, 2019). However, for **TFMP**, molecules should separate equally at the melting point on either side of a molecule. In **MOP**, molecules will separate first at the phenyl ends of the molecules while the methoxyphenyl ends would be predicted to persist into the liquid phase until enough energy was applied to overcome the 11 kJ mol^{-1} interaction energy (interaction #4).

6. Database survey

The Cambridge Structural Database was searched for possible crystal structures of these compounds. No entries were found for a crystal structure of *N*-[4-(trifluoromethyl)phenyl]benzamide. A room-temperature crystal structure was found for the *N*-(4-methoxyphenyl)benzamide compound (du Plessis *et al.*, 1983). The CIF file associated with this study, BUTDOJ, included only atom positions with no atomic displacement parameters. The *R* factor was listed as 0.106. In the published article, the authors noted that the overlapping reflections made it difficult to make an accurate background correction. This resulted, in the authors' words, 'in a somewhat poor set of intensity data for this compound'. For these reasons, we opted to use our redetermination of the crystal structure for the purpose of this publication.

7. Synthesis and crystallization

Details of the synthesis of the title compounds can be found in Chang *et al.* (2019). Product crystals for both compounds were grown by slow diffusion of hexanes into a concentrated solution of the amide in ethyl acetate.

8. Refinement

Crystal data, data collection and refinement details are summarized in Table 4. All hydrogen atoms were located in difference-Fourier maps. Final positions for most of the hydrogen atoms were calculated and included in a riding model relative to the bonded, non-hydrogen atoms by use of

Table 4
Experimental details.

	TFMP	MOP
Crystal data		
Chemical formula	$C_{14}H_{10}F_3NO$	$C_{14}H_{13}NO_2$
M_r	265.23	227.25
Crystal system, space group	Triclinic, $P\overline{1}$	Monoclinic, $P2_1/c$
Temperature (K)	173	173
a, b, c (Å)	5.3606 (11), 7.7831 (16), 14.415 (3)	26.7830 (15), 5.2477 (3), 8.1343 (5)
α, β, γ (°)	77.170 (7), 79.421 (7), 89.719 (7)	90, 97.594 (2), 90
V (Å^3)	576.0 (2)	1133.24 (11)
Z	2	4
Radiation type	Mo $K\alpha$	Mo $K\alpha$
μ (mm^{-1})	0.13	0.09
Crystal size (mm)	0.24 × 0.08 × 0.06	0.70 × 0.26 × 0.08
Data collection		
Diffractometer	Bruker APEXII CCD	Bruker APEXII CCD
Absorption correction	Multi-scan (*SADABS*; Bruker, 2018)	Multi-scan (*SADABS*; Bruker, 2018)
T_{min}, T_{max}	0.700, 1.000	0.518, 1
No. of measured, independent and observed [$I > 2\sigma(I)$] reflections	11667, 2201, 1415	36318, 2333, 1678
R_{int}	0.086	0.106
(sin $\theta/\lambda)_{max}$ (Å^{-1})	0.612	0.626
Refinement		
$R[F^2 > 2\sigma(F^2)]$, $wR(F^2)$, S	0.068, 0.189, 1.11	0.049, 0.126, 1.08
No. of reflections	2201	2333
No. of parameters	176	160
No. of restraints	1	1
H-atom treatment	H atoms treated by a mixture of independent and constrained refinement	H atoms treated by a mixture of independent and constrained refinement
$\Delta\rho_{max}$, $\Delta\rho_{min}$ (e Å^{-3})	0.26, −0.32	0.20, −0.19

Computer programs: *APEX3* and *SAINT* (Bruker, 2018), *SHELXT* (Sheldrick, 2015*a*), *SHELXL* (Sheldrick, 2015*b*), *WinGX* (Farrugia, 2012), *Mercury* (Macrae *et al.*, 2020), *CrystalExplorer17* (Spackman *et al.*, 2021), and *publCIF* (Westrip, 2010).

AFIX commands. Methyl hydrogen atoms were fixed at 0.98 Å from bonded carbon atoms, and phenyl hydrogen atoms were located 0.95 Å from bonded carbon atoms. Hydrogen displacement parameters were isotropic and set at 1.20 times the bonded phenyl carbons and 1.50 times the bonded methyl carbon in **MOP**. The amide hydrogens were treated differently because of their participation in the hydrogen bonding in these crystal structures. DFIX commands were set at 1.00 Å for these hydrogen atoms to allow for better comparison with the DFT-calculated N—H bond lengths. These hydrogen positions were then refined with independent isotropic displacement parameters. Isotropic extinction was refined in **MOP**. Although the 'standard' independent atom model was used for our analysis, alternative models were considered. Refinements with librationally corrected bond lengths and high-angle refinements were performed. These refinements had no significant effects on the structural results or the energy calculations.

Acknowledgements

The authors thank Megan Mohadjer Beromi of the Chemistry Department at USNA for reviewing the manuscript and offering helpful insights. We also thank Chip Nataro of Lafayette College for performing the CSD search.

Funding information

Funding for this research was provided by: Office of Naval Research (award No. N0001421WX01619 to DWLC); James Kinnear (USNA Class of 1950) (gift to SL, AHRM); Naval Academy Research Council (grant to SL, AHRM); DoD High Performance Modernization Program (award No. USNAM07923005 to JJU); USNA Faculty Enhancement Center (award to JJU, AHRM, and SL); USNA Faculty Development Fund (JJU, SL, and AHRM).

References

Banerjee, A., Saha, A. & Saha, B. K. (2019). *Cryst. Growth Des.* **19**, 2245–2252.
Blake, C. C. F. & Small, R. W. H. (1972). *Acta Cryst.* B**28**, 2201–2206.
Bruker (2018). *APEX3*, *SAINT* and *SADABS*. Bruker AXS Inc, Madison, Wisconsin, USA.
Chang, R. K., Clairmont, B. P., Lin, S. & MacArthur, A. H. R. (2019). *Organometallics*, **38**, 4448–4454.
Cruz-Cabeza, J. & Bernstein, J. (2014). *Chem. Rev.* **114**, 2170–2191.
Evano, G., Blanchard, N. & Toumi, M. (2008). *Chem. Rev.* **108**, 3054–3131.
Evano, G., Schaus, J. V. & Panek, J. S. (2004). *Org. Lett.* **6**, 525–528.
Farrugia, L. J. (2012). *J. Appl. Cryst.* **45**, 849–854.
Frisch, M. J., Trucks, G. W., Schlegel, H. B., Scuseria, G. E., Robb, M. A., Cheeseman, J. R., Scalmani, G., Barone, V., Mennucci, B., Petersson, G. A., Nakatsuji, H., Caricato, M., Li, X., Hratchian, H. P., Izmaylov, A. F., Bloino, J., Zheng, G., Sonnenberg, J. L., Hada, M., Ehara, M., Toyota, K., Fukuda, R., Hasegawa, J., Ishida, M., Nakajima, T., Honda, Y., Kitao, O., Nakai, H., Vreven, T.,

Montgomery, J. A., Jr., Peralta, J. E., Ogliaro, F., Bearpark, M., Heyd, J. J., Brothers, E., Kudin, K. N., Staroverov, V. N., Kobayashi, R., Normand, J., Raghavachari, K., Rendell, A., Burant, J. C., Iyengar, S. S., Tomasi, J., Cossi, M., Rega, N., Millam, J. M., Klene, M., Knox, J. E., Cross, J. B., Bakken, V., Adamo, C., Jaramillo, J., Gomperts, R., Stratmann, R. E., Yazyev, O., Austin, A. J., Cammi, R., Pomelli, C., Ochterski, J. W., Martin, R. L., Morokuma, K., Zakrzewski, V. G., Voth, G. A., Salvador, P., Dannenberg, J. J., Dapprich, S., Daniels, A. D., Farkas, Ö., Foresman, J. B., Ortiz, J. V., Cioslowski, J. & Fox, D. J. (2016). *GAUSSIAN 09*, Revision A. 02. Gaussian Inc., Wallingford CT, USA.

Greenberg, A., Brenemanm, C. M. & Liebman, J. F. (2000). *Amide Linkage: Selected Structural Aspects in Chemistry, Biochemistry, and Materials Science.* New York: Wiley-Interscience.

Groom, C. R., Bruno, I. J., Lightfoot, M. P. & Ward, S. C. (2016). *Acta Cryst.* B**72**, 171–179.

Jayatilaka, D. & Grimwood, D. J. (2003). *Computational Science|ICCS 2003*, edited by P. M. A. Sloot, D. Abramson, A. V. Bogdanov, Y. E. Gorbachev, J. J. Dongarra & A. Y. Zomaya, pp. 142–151. Berlin, Heidelberg: Springer.

Macrae, C. F., Sovago, I., Cottrell, S. J., Galek, P. T. A., McCabe, P., Pidcock, E., Platings, M., Shields, G. P., Stevens, J. S., Towler, M. & Wood, P. A. (2020). *J. Appl. Cryst.* **53**, 226–235.

Masse, C. E., Yang, M., Solomon, J. & Panek, J. S. (1998). *J. Am. Chem. Soc.* **120**, 4123–4134.

Plessis, M. P. du, Modro, T. A. & Nassimbeni, L. R. (1983). *J. Crystallogr. Spectrosc. Res.* **13**, 179–189.

Satyanarayana, K., Srinivas, K., Himabindu, V. & Reddy, G. M. (2007). *Org. Process Res. Dev.* **11**, 842–845.

Seward, N. & Jakubke, H. D. (2002). *Peptides: Chemistry and Biology.* Weinheim: Wiley-VCH.

Sheldrick, G. M. (2015*a*). *Acta Cryst.* A**71**, 3–8.

Sheldrick, G. M. (2015*b*). *Acta Cryst.* C**71**, 3–8.

Spackman, P. R., Turner, M. J., McKinnon, J. J., Wolff, S. K., Grimwood, D. J., Jayatilaka, D. & Spackman, M. A. (2021). *J. Appl. Cryst.* **54**, 1006–1011.

Spek, A. L. (2020). *Acta Cryst.* E**76**, 1–11.

Tanner, D., Fitzgerald, J. A. & Phillips, B. R. (1989). *Angew. Chem. Int. Ed. Engl.* **28**, 649–654.

Tothadi, S. & Desiraju, G. R. (2012). *Cryst. Growth Des.* **12**, 6188–6198.

Turner, M. J., Grabowsky, S., Jayatilaka, D. & Spackman, M. A. (2014). *J. Phys. Chem. Lett.* **5**, 4229–4255.

Wang, J.-L., Xu, J.-S., Wang, D.-Y., Wang, H., Li, Z.-T. & Zhang, D.-W. (2014). *CrystEngComm*, **16**, 2078–2084.

Wavefunction (2014). *SPARTAN*. Wavefunction Inc., Irvine, CA, USA.

Westrip, S. P. (2010). *J. Appl. Cryst.* **43**, 920–925.

Zhao, Y. & Truhlar, D. J. (2008). *Theor. Chem. Acc.* **120**, 215–241.

supporting information

Acta Cryst. (2022). E**78**, 297-305 [https://doi.org/10.1107/S2056989022000950]

Crystal structures of *N*-[4-(trifluoromethyl)phenyl]benzamide and *N*-(4-methoxyphenyl)benzamide at 173 K: a study of the energetics of conformational changes due to crystal packing

Wayne H. Pearson, Joseph J. Urban, Amy H. Roy MacArthur, Shirley Lin and Dylan W. L. Cabrera

Computing details

For both structures, data collection: *APEX3* (Bruker, 2018); cell refinement: *SAINT* (Bruker, 2018); data reduction: *SAINT* (Bruker, 2018); program(s) used to solve structure: SHELXT (Sheldrick, 2015a); program(s) used to refine structure: *WinGX* (Farrugia, 2012), *SHELXL* (Sheldrick, 2015b); molecular graphics: *Mercury* (Macrae *et al.*, 2020) and *CrystalExplorer17* Spackman *et al.*, 2021); software used to prepare material for publication: *publCIF* (Westrip, 2010).

N-[4-(Trifluoromethyl)phenyl]benzamide (1)

Crystal data

$C_{14}H_{10}F_3NO$
M_r = 265.23
Triclinic, $P\overline{1}$
a = 5.3606 (11) Å
b = 7.7831 (16) Å
c = 14.415 (3) Å
α = 77.170 (7)°
β = 79.421 (7)°
γ = 89.719 (7)°
V = 576.0 (2) Å^3
Z = 2
F(000) = 272
D_x = 1.529 Mg m^{-3}
D_m = 1.46 (2) Mg m^{-3}
D_m measured by flotation in K2CO3(aq) solution
Melting point = 477–478 K
Mo $K\alpha$ radiation, λ = 0.71073 Å
Cell parameters from 2253 reflections
θ = 2.7–23.2°
μ = 0.13 mm^{-1}
T = 173 K
Regular parallelpiped, colourless
0.24 × 0.08 × 0.06 mm

Data collection

Bruker APEXII CCD diffractometer
Radiation source: sealed X-ray tube
Detector resolution: 8.53 pixels mm^{-1}
rotating crystal scans
Absorption correction: multi-scan (*SADABS*; Bruker, 2018)
T_{min} = 0.700, T_{max} = 1.000
11667 measured reflections
2201 independent reflections
1415 reflections with $I > 2\sigma(I)$
R_{int} = 0.086
θ_{max} = 25.8°, θ_{min} = 1.5°
h = −6→6
k = −9→9
l = −17→17

Refinement

Refinement on F^2
Least-squares matrix: full
$R[F^2 > 2\sigma(F^2)] = 0.068$
$wR(F^2) = 0.189$
$S = 1.11$
2201 reflections
176 parameters
1 restraint
Primary atom site location: structure-invariant direct methods
Hydrogen site location: structure-invariant direct methods
H atoms treated by a mixture of independent and constrained refinement
$w = 1/[\sigma^2(F_o^2) + (0.0726P)^2 + 0.6085P]$ where $P = (F_o^2 + 2F_c^2)/3$
$(\Delta/\sigma)_{max} < 0.001$
$\Delta\rho_{max} = 0.26$ e Å^{-3}
$\Delta\rho_{min} = -0.32$ e Å^{-3}

Special details

Geometry. All esds (except the esd in the dihedral angle between two l.s. planes) are estimated using the full covariance matrix. The cell esds are taken into account individually in the estimation of esds in distances, angles and torsion angles; correlations between esds in cell parameters are only used when they are defined by crystal symmetry. An approximate (isotropic) treatment of cell esds is used for estimating esds involving l.s. planes.

Fractional atomic coordinates and isotropic or equivalent isotropic displacement parameters (Å²)

	x	*y*	*z*	U_{iso}*/U_{eq}
C1	0.4290 (8)	0.2664 (5)	0.9270 (3)	0.0361 (10)
C2	0.5101 (6)	0.2716 (5)	0.8223 (3)	0.0259 (8)
C3	0.3572 (6)	0.3479 (5)	0.7572 (3)	0.0274 (9)
H3	0.207249	0.403788	0.779424	0.033*
C4	0.4208 (6)	0.3432 (5)	0.6611 (3)	0.0269 (8)
H4	0.314467	0.395672	0.617458	0.032*
C5	0.6407 (6)	0.2620 (4)	0.6270 (2)	0.0228 (8)
C6	0.7958 (6)	0.1861 (5)	0.6926 (3)	0.0260 (8)
H6	0.947277	0.131744	0.670270	0.031*
C7	0.7301 (6)	0.1899 (5)	0.7885 (2)	0.0253 (8)
H7	0.834978	0.136384	0.832438	0.030*
C8	0.9209 (6)	0.2491 (5)	0.4709 (3)	0.0257 (8)
C9	0.9138 (6)	0.2390 (5)	0.3692 (3)	0.0238 (8)
C10	0.7131 (6)	0.1552 (5)	0.3439 (3)	0.0265 (8)
H10	0.572074	0.103421	0.392070	0.032*
C11	0.7225 (6)	0.1487 (5)	0.2481 (3)	0.0302 (9)
H11	0.587155	0.091657	0.230932	0.036*
C12	0.9254 (7)	0.2236 (5)	0.1773 (3)	0.0304 (9)
H12	0.928932	0.218903	0.111750	0.036*
C13	1.1249 (7)	0.3062 (5)	0.2021 (3)	0.0303 (9)
H13	1.265418	0.357914	0.153574	0.036*
C14	1.1180 (6)	0.3127 (5)	0.2979 (3)	0.0280 (9)
H14	1.255099	0.368467	0.314711	0.034*
F1	0.3071 (5)	0.4105 (3)	0.94336 (17)	0.0520 (7)
F2	0.6234 (5)	0.2548 (4)	0.97444 (18)	0.0599 (8)
F3	0.2713 (5)	0.1294 (4)	0.97311 (18)	0.0606 (8)
N1	0.6886 (5)	0.2533 (4)	0.5288 (2)	0.0253 (7)
O1	1.1224 (4)	0.2563 (4)	0.49980 (18)	0.0359 (7)
H1	0.541 (5)	0.261 (6)	0.495 (3)	0.052 (13)*

Atomic displacement parameters (Å²)

	U^{11}	U^{22}	U^{33}	U^{12}	U^{13}	U^{23}
C1	0.039 (2)	0.033 (2)	0.037 (2)	0.0094 (19)	−0.0088 (18)	−0.0111 (18)
C2	0.0212 (17)	0.027 (2)	0.030 (2)	0.0040 (15)	−0.0059 (15)	−0.0067 (16)
C3	0.0187 (17)	0.031 (2)	0.033 (2)	0.0076 (15)	−0.0031 (15)	−0.0104 (17)
C4	0.0178 (17)	0.030 (2)	0.036 (2)	0.0046 (15)	−0.0092 (15)	−0.0095 (16)
C5	0.0179 (16)	0.022 (2)	0.029 (2)	0.0015 (14)	−0.0057 (14)	−0.0065 (15)
C6	0.0159 (17)	0.032 (2)	0.031 (2)	0.0082 (15)	−0.0052 (14)	−0.0077 (16)
C7	0.0204 (17)	0.027 (2)	0.029 (2)	0.0061 (15)	−0.0095 (15)	−0.0031 (15)
C8	0.0196 (18)	0.026 (2)	0.032 (2)	0.0036 (14)	−0.0044 (15)	−0.0080 (16)
C9	0.0191 (17)	0.024 (2)	0.0293 (19)	0.0114 (14)	−0.0054 (14)	−0.0070 (15)
C10	0.0158 (16)	0.029 (2)	0.035 (2)	0.0062 (14)	−0.0043 (14)	−0.0084 (16)
C11	0.0206 (18)	0.034 (2)	0.040 (2)	0.0090 (16)	−0.0123 (16)	−0.0127 (17)
C12	0.029 (2)	0.037 (2)	0.030 (2)	0.0127 (17)	−0.0098 (16)	−0.0119 (17)
C13	0.0233 (19)	0.033 (2)	0.032 (2)	0.0101 (16)	−0.0007 (15)	−0.0054 (17)
C14	0.0180 (17)	0.032 (2)	0.036 (2)	0.0071 (15)	−0.0073 (15)	−0.0097 (17)
F1	0.0738 (18)	0.0462 (16)	0.0401 (14)	0.0300 (13)	−0.0083 (12)	−0.0207 (12)
F2	0.0573 (16)	0.093 (2)	0.0404 (15)	0.0265 (15)	−0.0240 (13)	−0.0268 (14)
F3	0.0735 (19)	0.0528 (17)	0.0442 (16)	−0.0077 (14)	0.0159 (13)	−0.0089 (12)
N1	0.0147 (14)	0.0351 (19)	0.0279 (17)	0.0076 (13)	−0.0064 (12)	−0.0093 (13)
O1	0.0162 (12)	0.062 (2)	0.0331 (15)	0.0062 (12)	−0.0074 (11)	−0.0161 (13)

Geometric parameters (Å, º)

C1—F3	1.335 (5)	C8—O1	1.233 (4)
C1—F2	1.340 (4)	C8—N1	1.370 (4)
C1—F1	1.340 (4)	C8—C9	1.493 (5)
C1—C2	1.484 (5)	C9—C14	1.384 (5)
C2—C3	1.391 (5)	C9—C10	1.405 (5)
C2—C7	1.397 (5)	C10—C11	1.385 (5)
C3—C4	1.373 (5)	C10—H10	0.9500
C3—H3	0.9500	C11—C12	1.378 (5)
C4—C5	1.396 (5)	C11—H11	0.9500
C4—H4	0.9500	C12—C13	1.391 (5)
C5—C6	1.403 (5)	C12—H12	0.9500
C5—N1	1.409 (4)	C13—C14	1.387 (5)
C6—C7	1.370 (5)	C13—H13	0.9500
C6—H6	0.9500	C14—H14	0.9500
C7—H7	0.9500	N1—H1	0.993 (10)
F3—C1—F2	105.9 (3)	O1—C8—N1	122.7 (3)
F3—C1—F1	106.1 (3)	O1—C8—C9	122.0 (3)
F2—C1—F1	105.7 (3)	N1—C8—C9	115.3 (3)
F3—C1—C2	112.7 (3)	C14—C9—C10	119.3 (3)
F2—C1—C2	113.1 (3)	C14—C9—C8	117.8 (3)
F1—C1—C2	112.7 (3)	C10—C9—C8	122.9 (3)
C3—C2—C7	119.0 (3)	C11—C10—C9	119.4 (3)

C3—C2—C1	120.0 (3)	C11—C10—H10	120.3
C7—C2—C1	120.9 (3)	C9—C10—H10	120.3
C4—C3—C2	120.7 (3)	C12—C11—C10	121.0 (3)
C4—C3—H3	119.7	C12—C11—H11	119.5
C2—C3—H3	119.7	C10—C11—H11	119.5
C3—C4—C5	120.5 (3)	C11—C12—C13	119.8 (3)
C3—C4—H4	119.8	C11—C12—H12	120.1
C5—C4—H4	119.8	C13—C12—H12	120.1
C4—C5—C6	118.9 (3)	C14—C13—C12	119.7 (3)
C4—C5—N1	117.8 (3)	C14—C13—H13	120.1
C6—C5—N1	123.3 (3)	C12—C13—H13	120.1
C7—C6—C5	120.4 (3)	C9—C14—C13	120.8 (3)
C7—C6—H6	119.8	C9—C14—H14	119.6
C5—C6—H6	119.8	C13—C14—H14	119.6
C6—C7—C2	120.6 (3)	C8—N1—C5	127.0 (3)
C6—C7—H7	119.7	C8—N1—H1	115 (3)
C2—C7—H7	119.7	C5—N1—H1	117 (3)

Hydrogen-bond geometry (Å, º)

D—H···*A*	*D*—H	H···*A*	*D*···*A*	*D*—H···*A*
C6—H6···O1	0.95	2.44	2.938 (4)	112
C4—H4···O1^{i}	0.95	2.57	3.240 (4)	128
N1—H1···O1^{i}	0.99 (1)	2.23 (2)	3.138 (3)	151 (3)

Symmetry code: (i) *x*−1, *y*, *z*.

N-(4-Methoxyphenyl)benzamide (2)

Crystal data

$C_{14}H_{13}NO_2$
M_r = 227.25
Monoclinic, $P2_1/c$
a = 26.7830 (15) Å
b = 5.2477 (3) Å
c = 8.1343 (5) Å
β = 97.594 (2)°
V = 1133.24 (11) Å^3
Z = 4
F(000) = 480
D_x = 1.332 Mg m^{-3}
D_m = 1.29 (2) Mg m^{-3}
D_m measured by flotation in aqueous KI
Melting point = 424–425 K
Mo $K\alpha$ radiation, λ = 0.71073 Å
Cell parameters from 5514 reflections
θ = 3.1–26.0°
μ = 0.09 mm^{-1}
T = 173 K
Regular parallelpiped, colourless
0.70 × 0.26 × 0.08 mm

Data collection

Bruker APEXII CCD diffractometer
Radiation source: sealed X-ray tube
Detector resolution: 8.53 pixels mm^{-1}
rotating crystal scans
Absorption correction: multi-scan (*SADABS*; Bruker, 2018)
T_{min} = 0.518, T_{max} = 1
36318 measured reflections
2333 independent reflections
1678 reflections with $I > 2\sigma(I)$
R_{int} = 0.106
θ_{max} = 26.4°, θ_{min} = 1.5°
h = −33→33
k = −6→6
l = −10→10

Refinement

Refinement on F^2
Least-squares matrix: full
$R[F^2 > 2\sigma(F^2)] = 0.049$
$wR(F^2) = 0.126$
$S = 1.08$
2333 reflections
160 parameters
1 restraint
Primary atom site location: structure-invariant direct methods
Hydrogen site location: structure-invariant direct methods
H atoms treated by a mixture of independent and constrained refinement
$w = 1/[\sigma^2(F_o^2) + (0.0247P)^2 + 0.8083P]$ where $P = (F_o^2 + 2F_c^2)/3$
$(\Delta/\sigma)_{max} = 0.001$
$\Delta\rho_{max} = 0.20$ e Å^{-3}
$\Delta\rho_{min} = -0.19$ e Å^{-3}
Extinction correction: SHELXL-2018/3 (Sheldrick, 2015b), $Fc^* = kFc[1+0.001xFc^2\lambda^3/\sin(2\theta)]^{-1/4}$
Extinction coefficient: 0.0099 (18)

Special details

Geometry. All esds (except the esd in the dihedral angle between two l.s. planes) are estimated using the full covariance matrix. The cell esds are taken into account individually in the estimation of esds in distances, angles and torsion angles; correlations between esds in cell parameters are only used when they are defined by crystal symmetry. An approximate (isotropic) treatment of cell esds is used for estimating esds involving l.s. planes.

Refinement. isotropic extinction correction applied

Fractional atomic coordinates and isotropic or equivalent isotropic displacement parameters (Å²)

	x	*y*	*z*	U_{iso}*/U_{eq}
C1	0.53199 (8)	0.7401 (5)	0.1647 (3)	0.0544 (7)
H1A	0.529249	0.745250	0.283557	0.082*
H1B	0.498295	0.724788	0.101786	0.082*
H1C	0.547952	0.897114	0.132379	0.082*
C2	0.61069 (7)	0.5196 (4)	0.2084 (2)	0.0350 (5)
C3	0.63993 (8)	0.3201 (4)	0.1635 (3)	0.0388 (5)
H3	0.625795	0.197660	0.084749	0.047*
C4	0.68972 (8)	0.2992 (4)	0.2334 (3)	0.0369 (5)
H4	0.709605	0.161154	0.203434	0.044*
C5	0.71075 (7)	0.4793 (4)	0.3471 (2)	0.0319 (4)
C6	0.68127 (8)	0.6755 (4)	0.3937 (3)	0.0362 (5)
H6	0.695284	0.796302	0.473747	0.043*
C7	0.63122 (7)	0.6971 (4)	0.3240 (3)	0.0361 (5)
H7	0.611137	0.833235	0.355679	0.043*
C8	0.79514 (7)	0.6427 (4)	0.4517 (3)	0.0367 (5)
C9	0.84768 (7)	0.5666 (4)	0.5223 (3)	0.0343 (5)
C10	0.85869 (8)	0.3512 (4)	0.6189 (3)	0.0412 (5)
H10	0.832343	0.240278	0.640884	0.049*
C11	0.90810 (9)	0.2974 (5)	0.6833 (3)	0.0493 (6)
H11	0.915465	0.151421	0.751318	0.059*
C12	0.94644 (9)	0.4548 (5)	0.6491 (3)	0.0502 (6)
H12	0.980294	0.416164	0.692292	0.060*
C13	0.93588 (8)	0.6682 (5)	0.5525 (3)	0.0495 (6)
H13	0.962451	0.776471	0.528736	0.059*
C14	0.88664 (8)	0.7252 (4)	0.4899 (3)	0.0417 (5)
H14	0.879440	0.873678	0.424217	0.050*

N1	0.76211 (6)	0.4491 (3)	0.4173 (2)	0.0358 (4)
O2	0.56174 (5)	0.5266 (3)	0.13011 (19)	0.0477 (4)
O1	0.78412 (6)	0.8674 (3)	0.4262 (2)	0.0572 (5)
H1	0.7748 (8)	0.277 (2)	0.424 (3)	0.041 (6)*

Atomic displacement parameters (Å²)

	U^{11}	U^{22}	U^{33}	U^{12}	U^{13}	U^{23}
C1	0.0349 (12)	0.0616 (16)	0.0642 (17)	0.0071 (11)	−0.0026 (11)	−0.0003 (13)
C2	0.0296 (10)	0.0395 (11)	0.0348 (11)	−0.0032 (9)	0.0001 (8)	0.0042 (9)
C3	0.0404 (12)	0.0366 (12)	0.0377 (12)	−0.0039 (9)	−0.0014 (9)	−0.0053 (9)
C4	0.0365 (11)	0.0321 (11)	0.0420 (12)	0.0014 (9)	0.0053 (9)	−0.0020 (9)
C5	0.0310 (10)	0.0309 (10)	0.0334 (11)	−0.0017 (8)	0.0024 (8)	0.0033 (8)
C6	0.0347 (11)	0.0341 (11)	0.0382 (12)	−0.0002 (9)	−0.0010 (9)	−0.0050 (9)
C7	0.0323 (11)	0.0356 (11)	0.0402 (12)	0.0021 (9)	0.0044 (9)	−0.0026 (9)
C8	0.0331 (11)	0.0313 (11)	0.0447 (13)	0.0016 (9)	0.0020 (9)	−0.0001 (9)
C9	0.0321 (11)	0.0316 (10)	0.0380 (11)	0.0013 (8)	0.0007 (9)	−0.0042 (9)
C10	0.0410 (12)	0.0359 (12)	0.0449 (13)	−0.0010 (9)	−0.0010 (10)	0.0002 (10)
C11	0.0505 (14)	0.0432 (13)	0.0504 (14)	0.0103 (11)	−0.0079 (11)	0.0015 (11)
C12	0.0349 (12)	0.0584 (15)	0.0539 (15)	0.0113 (11)	−0.0066 (10)	−0.0111 (12)
C13	0.0336 (12)	0.0557 (15)	0.0576 (15)	−0.0045 (11)	0.0009 (10)	−0.0062 (12)
C14	0.0365 (11)	0.0394 (12)	0.0479 (13)	−0.0023 (9)	0.0011 (10)	0.0016 (10)
N1	0.0297 (9)	0.0281 (9)	0.0479 (11)	0.0017 (7)	−0.0014 (7)	0.0007 (8)
O2	0.0301 (8)	0.0552 (10)	0.0548 (10)	0.0004 (7)	−0.0060 (7)	−0.0063 (8)
O1	0.0376 (9)	0.0302 (8)	0.0996 (14)	0.0016 (7)	−0.0063 (9)	0.0055 (9)

Geometric parameters (Å, º)

C1—O2	1.424 (3)	C8—O1	1.227 (2)
C1—H1A	0.9800	C8—N1	1.352 (3)
C1—H1B	0.9800	C8—C9	1.502 (3)
C1—H1C	0.9800	C9—C10	1.386 (3)
C2—O2	1.380 (2)	C9—C14	1.387 (3)
C2—C7	1.385 (3)	C10—C11	1.387 (3)
C2—C3	1.385 (3)	C10—H10	0.9500
C3—C4	1.383 (3)	C11—C12	1.375 (3)
C3—H3	0.9500	C11—H11	0.9500
C4—C5	1.389 (3)	C12—C13	1.376 (3)
C4—H4	0.9500	C12—H12	0.9500
C5—C6	1.381 (3)	C13—C14	1.382 (3)
C5—N1	1.426 (2)	C13—H13	0.9500
C6—C7	1.389 (3)	C14—H14	0.9500
C6—H6	0.9500	N1—H1	0.965 (10)
C7—H7	0.9500		
O2—C1—H1A	109.5	O1—C8—C9	120.83 (18)
O2—C1—H1B	109.5	N1—C8—C9	115.72 (17)
H1A—C1—H1B	109.5	C10—C9—C14	119.21 (19)

O2—C1—H1C	109.5	C10—C9—C8	123.50 (19)
H1A—C1—H1C	109.5	C14—C9—C8	117.28 (19)
H1B—C1—H1C	109.5	C9—C10—C11	120.1 (2)
O2—C2—C7	124.29 (19)	C9—C10—H10	119.9
O2—C2—C3	115.73 (18)	C11—C10—H10	119.9
C7—C2—C3	119.98 (18)	C12—C11—C10	120.1 (2)
C4—C3—C2	119.97 (19)	C12—C11—H11	119.9
C4—C3—H3	120.0	C10—C11—H11	119.9
C2—C3—H3	120.0	C11—C12—C13	120.1 (2)
C3—C4—C5	120.28 (19)	C11—C12—H12	119.9
C3—C4—H4	119.9	C13—C12—H12	119.9
C5—C4—H4	119.9	C12—C13—C14	120.0 (2)
C6—C5—C4	119.58 (18)	C12—C13—H13	120.0
C6—C5—N1	121.95 (18)	C14—C13—H13	120.0
C4—C5—N1	118.42 (18)	C13—C14—C9	120.4 (2)
C5—C6—C7	120.34 (19)	C13—C14—H14	119.8
C5—C6—H6	119.8	C9—C14—H14	119.8
C7—C6—H6	119.8	C8—N1—C5	124.71 (17)
C2—C7—C6	119.81 (19)	C8—N1—H1	118.4 (13)
C2—C7—H7	120.1	C5—N1—H1	116.2 (13)
C6—C7—H7	120.1	C2—O2—C1	116.87 (17)
O1—C8—N1	123.44 (19)		

Hydrogen-bond geometry (Å, º)

D—H···*A*	*D*—H	H···*A*	*D*···*A*	*D*—H···*A*
C6—H6···O1	0.95	2.49	2.912 (2)	107
N1—H1···O1^{i}	0.96 (1)	2.16 (1)	3.108 (2)	166 (2)

Symmetry code: (i) *x*, *y*−1, *z*.